LA-UR-16-26398
Approved for public release; distribution is unlimited.

Title: Advanced Sensor Arrays and Packaging

Author(s): Ryter, John Wesley

Intended for: Report

Issued: 2016-08-19

# Advanced Sensor Arrays and Packaging

John Ryter, Christopher J. Romero, Kannan Ramaiyan, Eric L. Brosha

Office of Science, Science Undergraduate Laboratory Internship (SULI)
Los Alamos National Laboratory, Materials Synthesis and Integrated Devices Group
Los Alamos, NM 87545, United States

August 11, 2016

Prepared in partial fulfillment of the requirements of the Office of Science, Department of Energy's Science Undergraduate Laboratory Internship under the direction of Dr. Eric Brosha in the Materials Synthesis and Integrated Devices Group, Los Alamos National Laboratory

# TABLE OF CONTENTS


ABSTRACT **ii**

1.0 INTRODUCTION **1**

2.0 MATERIALS AND METHODS **2**
*2.1 Automotive Diagnostics Sensor Packaging* *2*
2.1.a Design Goals and Constraints 2
2.1.b Final Design and Production 3
*2.2 Sensor Arrays and Packaging* *4*
2.2.a Design Goals and Constraints 4
2.2.b Final Design and Production 5
*2.3 Hydrogen Sensor Field Trials Deployment* *5*
2.3.1 Electrode Material Comparison for New Installation 5
2.3.2 Data Analysis of Current Field Trials 6

**3.0 Results** **6**
*3.1 Automotive Diagnostic Sensor Packaging* *6*
*3.2 Sensor Arrays and Packaging* *6*
*3.3 Hydrogen Sensor Field Trials Deployment* *7*
3.3.1 Electrode Material Comparison for New Installation 7
3.3.2 Data Analysis of Current Field Trials 7

**4.0 Conclusions** **8**

**5.0 Figures** **9**

**Acknowledgements** **19**

ABSTRACT

Novel sensor packaging elements were designed, fabricated, and tested in order to facilitate the transition of electrochemical mixed-potential sensors toward commercialization. Of the two designs completed, the first is currently undergoing field trials, taking direct measurements within vehicle exhaust streams, while the second is undergoing preliminary laboratory testing. The sensors' optimal operating conditions, sensitivity to hydrogen, and long-term baseline stability were also investigated. The sensing capabilities of lanthanum chromite ($La_{0.8}Sr_{0.2}CrO_3$) and indium-doped tin oxide (ITO) working electrodes were compared, and the ITO devices were selected for pre-commercial field trials testing at a hydrogen fuel cell vehicle fueling station in California. Previous data from that fueling station were also analyzed, and the causes of anomalous baseline drift were identified.

## 1.0 INTRODUCTION

Mixed potential electrochemical sensors develop a non-Nernstian electric potential when equilibrated with an atmosphere containing an oxidizing or reducing gas.[1,2] Mixed potential devices consist of an oxygen ion conducting electrolyte and metal/metal oxide electrodes, where the choice of electrode materials is dependent on differences in the redox reaction kinetics at each electrode/electrolyte gas interface. Pairing electrodes with fast (Pt) and slow (Au, chromite ($LaCrO_3$), or indium tin oxide (ITO)) oxygen reduction kinetics enables sensitivity to a wide range of oxidizing and reducing gases, including hydrogen ($H_2$), nitrogen oxide ($NO_x$) species, ammonia ($NH_3$), and hydrocarbons (HCs).[3] The magnitude of the voltage response is dependent on the concentration of the reactant gas, reaction kinetics, gas composition, electrode/electrolyte composition and morphology, and operating temperature. As a result, these sensors may be selectively tuned to sense specific gas species with minimal cross-interference, which has been accomplished using current biasing, operating temperature controls, and differing electrode materials.[4] Additionally, multiple sensors operating at different temperatures enable the deconvolution of complex gas mixtures also improve the accuracy of single-gas detection.[5] These sensors have potential commercial applications in the automotive industry, in explosives detection and identification, and as hydrogen safety sensors. They are also simple in design and construction, inexpensive to manufacture, and robust due to their close relationship to the ubiquitous automotive Lambda sensor.[6] The sensors developed at Los Alamos Laboratory have taken two forms – the stick sensor design and the four-post sensor design– each with a different application and design considerations (Figure 1).

Current state-of-the-art automotive sensors use infrared technology, requiring that gases be removed from the exhaust stream and transported to a sampling cell, where the gas traces from all of the engine cylinders are collected for analysis. This averaging technique is slow and inaccurate, impeding the precise diagnostics required by today's increasingly advanced engine technologies.[7] As emissions regulations become more stringent, necessitating the advancement of complex emissions control technologies, diesel engines in particular require real-time $NO_x$, $NH_3$, and HC sensors to control injection rates of exhaust treatment fluids in a closed loop system.[8] Mixed-potential electrochemical sensors have the capacity to satisfy these needs, and this paper discusses the recent progress in developing and testing commercially viable sensor and sensor packaging designs. Previous research has focused on testing and validating these LANL-developed sensors in both diesel and lean burn gasoline exhaust streams at the National Transportation Research Center (NTRC) at Oak Ridge National Laboratory (ORNL), while this work has developed novel packaging elements currently undergoing testing at Automotive Test Solutions (ATS) in Albuquerque, New Mexico. These novel packaging designs sought to facilitate the transition toward real-world testing and commercialization, replacing the laboratory testing methods shown in Figure 2.

Although these sensors can be selectively tuned, cross-interference often occurs in complex gas mixtures where other oxidizing or reducing agents are present. However, the use of multiple differently tuned sensors can allow for the deconvolution of complex gas mixtures. Previous work has shown that a single sensor is capable of deconvoluting a two-gas mixture when paired with the Bayesian statistical models developed through collaboration with mathematicians at Rutger's University.[9] By developing a large data set consisting of various gases and gas concentrations, the Bayesian framework can be generalized and applied to the sensor voltage readings, allowing predictions of absolute gas concentrations.[10] Data collection is ongoing that will enable a four-sensor array, and a packaging element was produced capable of facilitating the transition of this technology toward commercialization.

Gaseous hydrogen has a variety of applications, from the manufacture of fertilizer to future fuel for fuel cell vehicles (FCVs) and rocket propellant, all requiring the use of robust safety sensors due to hydrogen's ease of combustion. With the advent of FCVs, which bring large volumes of hydrogen in close proximity to major population centers, an inexpensive and highly responsive safety sensor is imperative.[11] Because hydrogen is a reductant, the LANL-developed electrochemical sensors have been investigated for use as hydrogen safety sensors as well. Two sensors were installed at a hydrogen fuelling station in California earlier this year – one at the dispenser and one at the compressor skid – and their operation has been recorded and compared with that of the commercial safety sensors operating onsite. The LANL-developed sensors have shown significantly higher sensitivity than the industry standard sensors, but minor issues with their operation have been identified and will be addressed. All of the sensors developed at LANL have demonstrated logarithmic responses. Sensor saturation occurs when the oxidation-reduction reactions at the electrodes can no longer progress, resulting in indistinguishable responses for all gas concentrations above the saturation threshold. Methods of increasing this threshold will be discussed. Additionally, indium-doped tin oxide (ITO) and lanthanum chromite ($La_{0.8}Sr_{0.2}CrO_3$) were investigated and compared as potential working electrode materials.

## 2.0 MATERIALS AND METHODS

### 2.1 Automotive Diagnostics Sensor Packaging

#### *2.1.a Design Goals and Constraints*

In order to maximize the ease of commercialization and minimize production costs, each design was tailored to mesh seamlessly with readily available commercial products. This project was also undertaken in collaboration with Automotive Test Solutions, an Albuquerque-based company, and consequently the compatibility of these designs with their testing components and practices was also considered. The overarching goal of this project was to design a sensor-packaging element that would enable the LANL-developed stick sensor to operate in an

automotive setting, particularly within a gasoline or diesel engine exhaust pipe. To facilitate commercialization, the sensor had to be operable by mechanics and other industrial workers, with minimal training in the sensor's use. The stick sensor, though being larger than the four-post sensor, was selected due to its more robust construction and wiring methods. With these constraints, the sensor, including its packaging, was required to be low profile, robust, and versatile.

The size of the packaging was minimized such that the sensor could be inserted directly into a vehicle exhaust pipe. The number of edges and other protruding elements also required minimization to ensure the packaging would not be caught on any surfaces within the exhaust pipe. Operation within an exhaust stream would also pose a threat to the sensor due to particulate bombardment, and consequently protection was required that would block particles while still allowing non-turbulent flow. The previous packaging design also suffered from leakage due to the use of a press fit, which kept its two halves from separating, and consequently leakage minimization was considered. The overall fragility of the sensor itself necessitated further protection, including vibration minimization and shock absorption.

Several temperature considerations were also required. All materials, including the packaging as well as the associated wires and their insulation, had to withstand exhaust gas temperatures of up to 250°C (as shown by dynamometer data collected at ORNL), as well as the consequent thermal stresses and stresses incited by thermal expansion. Vibration resistance also required consideration, because the sensor needed to be held in place such that all wire contact points would remain constant while in contact with a vibrating tailpipe, regardless of thermal expansion or contraction. The conductivity, reactivity, thermal limits and expansion, and pliability of the utilized materials were also considered.

*2.1.b Final Design and Production*

To both hold and protect the sensor, a sensor holder and a sensor cover were designed as shown in Figures 3 and 4. For ease of manufacturing and assembly, these two components were designed to fit into each other with a sliding tolerance, allowing for less precision in manufacturing than an interference fit. Similar to a standard automotive oxygen sensor holder, the holder was designed such that applied compression would keep the sensor in place, with the same concept applied to the sensor cover as well. Hence, the assembly was designed to be held together by a single clamp, as shown in Figure 5, which also showcases the final design. Because none of the materials under consideration for these applications were flexible enough to be compressed by the relatively small forces applied by a clamp, slits were incorporated into the design of both components to allow torques rather than direct compression to induce holding forces.

Size, vibration resistance, and manufacturability were the primary constraints for the selection of the proper compression fitting. Previous LANL sensor packaging designs, used for R&D purposes, have relied on setscrews to both maintain contact with the heater and electrode pads and hold the sensor in place. This design, however, was found to be only minimally resistant to vibration as well

as incapable of providing the forces required to compress both the sensor cover and sensor holder. The direct installation of setscrews would have added additional manufacturing difficulties as well. Various other commercial compression fittings were investigated, including vibration-resistant pinch clamps and vibration-resistant worm-drive clamps, shown in Figure 6. Although the worm-drive clamps allowed for the greatest flexibility and ease of assembly, the protrusion of the worm screw increased the width of the packaging by more than 0.3 inches (approximately 68%), resulting in its disqualification. The pinch clamps, on the other hand, added a total width of approximately 0.062 inches (approximately 14%) at their widest point. Though they were found to be far more difficult to remove, they were selected due to their significant size advantages. Double pinch clamps were selected over single pinch clamps because they allowed for a wider range of diameters and allowed for greater, more evenly distributed compression forces to be applied.

Polyether ether ketone (PEEK) plastic was selected as the sensor holder material due to its lack of electrical conductivity, high melting point (334°C), corrosion resistance, and availability.[12] Stainless steel was selected for the sensor cover and pinch clamps due to its high corrosion resistance and availability. Teflon (polytetrafluoroethylene or PTFE)-coated wiring was selected for power and signal transmission due to its high temperature resistance. To connect the sensor holder assembly to the ATS-supplied flexible hosing, the sensor holder was designed to incorporate standard stainless steel Swagelok components, further enabling an easy transition toward commercialization.

## 2.2 Sensor Arrays and Packaging

### *2.2.a Design Goals and Constraints*

In order to simplify and downsize the existing sensor array testing assembly (Figure 7), this design necessitated the incorporation of at least four sensors in the smallest space possible, with the goal of enabling more straightforward laboratory testing and eventually field trials. The array element was required to fit inside a 0.870-inch inside diameter quartz tube, which would be used for laboratory testing, while also maintaining sufficient distance between the heaters and the packaging element to minimize the introduction of thermal stresses or melting of the selected material. The wire coatings used to power the sensor heaters and transmit the sensor responses also required protection from the high temperatures produced by the sensor heaters. This design also necessitated incorporation with threaded tubing, which would both hold the sensor in place and house the wiring.

As a further means of minimization, this design sought to decrease the number of power supplies required to operate the four-sensor array. The previous testing setup required a power supply for each sensor because each heater must operate at a different temperature, necessitating different heater voltages. In seeking to power the sensor array using a single power supply, a variety of circuit designs were considered that would result in each heater operating at sufficiently different temperatures. These circuit designs were constrained by the voltage and current limits of the power supplies as well as the size and power capacity of the

associated resistors. As this design progresses toward commercialization, additional design constraints will be required, including vibration minimization, shock absorption, and the incorporation of all circuitry directly into the array assembly.

### *2.2.b Final Design and Production*

The four-post sensors were utilized in a planar configuration to minimize the size of the assembly and evenly distribute gas flow. Because the four-post sensors require mounting on pins, a non-conductive, high-temperature material was required for mounting the sensors. As a result, PEEK plastic was selected early in the design process. Its high melting temperature enabled the sensors to be mounted closer to the sensor platform, permitting greater flexibility in the design. Taking advantage of this greater flexibility, the platform was designed such that the pins would protrude from both sides, enabling mounting of the sensors on one side and wiring on the other. This separation kept the wiring side at a significantly lower temperature, allowing the use of super glue for securing the pins in place and low-cost nylon-coated wiring for all connections. The pins were placed so as to minimize the size of the platform while still allowing clearance for the wire wrapping and soldering required to attach the sensors. The utilization of these low-temperature and commercially available components further advanced the economic feasibility of this design.

In order to comply with the voltage and current capacities of the power supply, the circuit shown in Figure 8a was selected. Other, more traditional designs incorporated a resistor in parallel or in series with each heater, and each pair then in series (Figure 8b) or in parallel (Figure 8c) with the rest. These two designs were more demanding on the power supply, and consequently were not selected. By maintaining the lower power requirements, the final circuit design also better protected the full array of sensor heaters from burning out in the case of a singular heater failure. The final circuit design also reduced the number of resistors required from four to two, resulting in a simpler and more robust configuration.

## 2.3 Hydrogen Sensor Field Trials Deployment

### *2.3.1 Electrode Material Comparison for New Installation*

Two hydrogen sensor electrode materials were compared, with the end result being installation at a hydrogen fueling station in Burbank, California. Each sensor type maintained the same materials and basic design, but the material on one electrode was varied, with either lanthanum chromite or ITO being used. The testing procedures for both sensors were the same. Initially the sensors were tested using a fixed power supply. The optimal voltage for each sensor heater was determined by computing the heater resistance during operation, then using its nominal resistance to compute its operating temperature using the plot shown in Figure 9. In most cases, the optimal voltage was the highest that could be attained without burning

out the heater, because higher sensor operating temperatures were found correspond with higher saturation thresholds.

Once the optimal heater voltages were established, the sensors were subjected to a variety of hydrogen staircase challenges such as that shown in Figure 10. These tests were performed using both the fixed power supply and with the power supplies used in the field, designated by the CRPS-PHIB series and manufactured by Custom Sensor Solutions. After a sufficient number of tests had been performed, a calibration curve was developed for each sensor, which was used to check the reproducibility of the sensor response. Finally, the sensors were placed in the wall-mounted field trials sensor enclosure (Figure 11) that was eventually installed at another hydrogen fueling station, where they were subjected to further challenges and testing.

### *2.3.2 Data Analysis of Current Field Trials*

Following data transmission from the two hydrogen fueling center sensors, a number of variables were investigated to determine the causes of a longstanding issue. Both sensors have displayed cyclic baseline drift with a period of approximately 24 hours as shown in Figure 12, indicating environmental causes. Consequently the weather data collected on-site, including the temperature, humidity, and barometric pressure, were plotted alongside the sensor baseline response in hopes of manifesting a correlation. The fueling station also supplied its fueling records, which were incorporated into the dataset as shown in Figure 13. The compressor skid sensor was bypassed during its installation, and consequently all data recorded for its response was a result only of the associated electronics.

## **3.0 Results**

### 3.1 Automotive Diagnostic Sensor Packaging

The final design is shown in Figure 5, showing the full assembly and incorporation into industry-standard technology. The collaboration with ATS has enabled a rapid transition toward full-scale commercialization. If the current testing is successful, they aim to facilitate the production of 800 to 1000 of these sensors and sensor packaging elements for distribution throughout New Mexico, enabling significant improvements in engine diagnostics technology.

### 3.2 Sensor Arrays and Packaging

The full design is shown in Figure 14, and the final product with mounted sensors is shown in Figure 15. As shown, five sensors were incorporated into the final design, allowing for the sensor array to be used in even more complex gas mixtures in the future as well as providing a backup sensor for its present

application. The final assembly is shown in Figure 16, which displays the incorporation of the final circuit design, the single heater power supply, and the standard mounting procedure. The wiring for the two resistors used to induce separate sensor operating temperatures was performed outside the main array assembly, allowing for a non-permanent resistor setup and enabling greater flexibility as the sensor operating conditions are fine-tuned in the future. The heater on sensor 2, the sensor operating at the highest temperature, burned out during preliminary baseline testing. Although this failure should have increased the voltage applied to the remaining sensors, the circuit design and feedback response of the power supply kept the other heaters from burning out as well.

## 3.3 Hydrogen Sensor Field Trials Deployment

### *3.3.1 Electrode Material Comparison for New Installation*

The lanthanum chromite sensors demonstrated significantly higher hydrogen saturation thresholds than the ITO sensors, as shown in Figure 17. The higher thresholds exhibited in the lanthanum chromite sensors, being near the lower flammability limit for hydrogen (4% by volume, or 40,000 ppm), established these sensors as promising candidates for commercial hydrogen safety sensors. However, significant exposure to hydrogen induced an anomalous reduced response in the lanthanum chromite sensors, as shown in Figure 18. While this reduced response would not inhibit the standard operation of a lanthanum chromite-based safety sensor – the detection of a leak when it first occurs – the occurrence of a large, prolonged leak could eventually oversaturate the sensor, causing its response to drop and potentially resulting in a false negative. As a result the lanthanum chromite sensors were not recommended for field trials testing, or for further use as hydrogen safety sensors. The ITO sensors, despite having very low saturation thresholds, showed reproducible responses as well as high sensitivity, and consequently ITO sensors were installed in Burbank and Chino, CA.

### *3.3.2 Data Analysis of Current Field Trials*

Data analysis showed continuation of the previously observed baseline drift for both sensor response channels, and the occurrence of extreme weather conditions – namely temperatures exceeding 43˚C (110˚F) – further exacerbated its effects, as shown in Figure 19. The two sensor response channels mirrored each other in their baseline drift, indicating that because the compressor skid sensor had been bypassed during its installation, the drift was due only to the influence of the associated electronics. Despite the cyclic drift, however, analysis of its maxima and minima over a sixty-day period indicated no overall drift in the sensor response, as shown in Figure 20. Additionally, nearly every peak in the dispenser sensor's response was correlated with a hydrogen vehicle-fueling event (Figure 13), with the remainder of those peaks correlating with other controlled releases not recorded in the vehicle fueling records.

## 4.0 Conclusions

The automotive diagnostic sensor assembly was found to be largely successful in terms of its low-cost and simple construction, though the ATS field trials testing will demonstrate whether it is successful in real-world testing. If it is successful, small refinements may be made but the transition toward commercialization will begin in earnest. Future work may include the removal of the slots at the end of the sensor holder, as they were not utilized in the final assembly and their removal would reduce future manufacturing costs.

The sensor array was also largely successful, but wiring difficulties did occur. In future designs, however, any necessary resistors will be incorporated into the main array assembly, further reducing the number of wires required to enter and exit the metal tubing. Tubing with a larger inside diameter is recommended, but it is not necessary for the successful assembly of the product. Future work will involve rewiring the array assembly to bypass the burned-out sensor, making use of the backup sensor as its replacement. The failure of the burned-out sensor must also be investigated further by analyzing the operating characteristics of the power supply. In order for the sensor array to be used in real-world testing scenarios, a cover will be required to shield it from particulates. Because of the size required, its influence on the development of turbulent flow should be a primary design consideration.

The ITO sensor was shown to be the more reliable of the two sensors tested, and consequently an ITO sensor was used to replace one of the two lanthanum chromite sensors for the Burbank field trials, enabling the direct comparison of the lanthanum chromite and ITO sensors under real-world conditions. The low saturation threshold in the ITO sensor – its primary drawback – will be further investigated, with electrode geometry being a primary consideration. Additional work will result in the development of a software or hardware system to mitigate the drift induced by the power supply electronics.

## 5.0 Figures

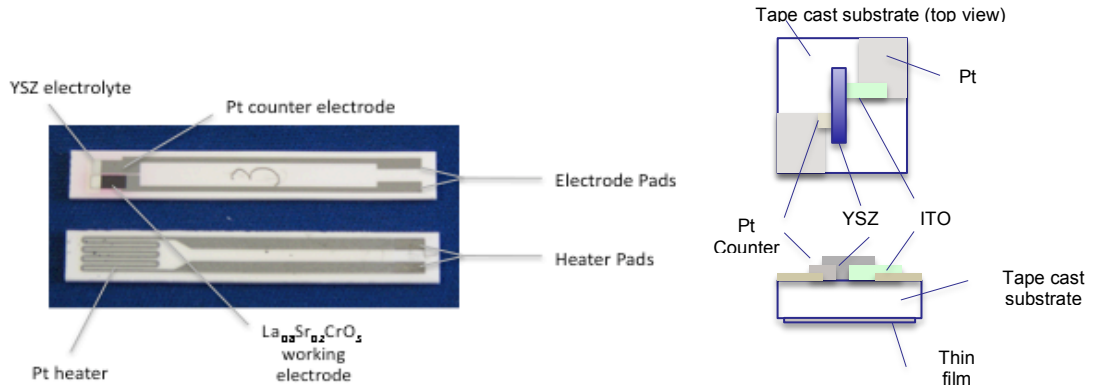


(a) (b)

FIG. 1. (a) The LANL-developed stick sensor, with each component labeled. (b) A rendering of the LANL-developed four-post sensor, with each component labeled.

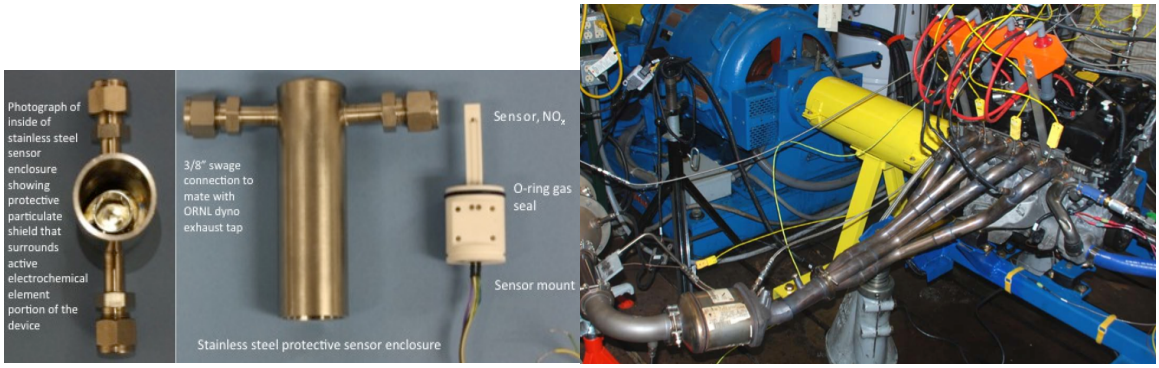


(a) (b)

FIG. 2. (a) The standard laboratory testing enclosure, which must be incorporated into a flow stream using additional tubing. (b) Large simulated engine platforms, such as that at ORNL, are used to replicate real-world testing conditions and enable the incorporation of laboratory testing enclosures.

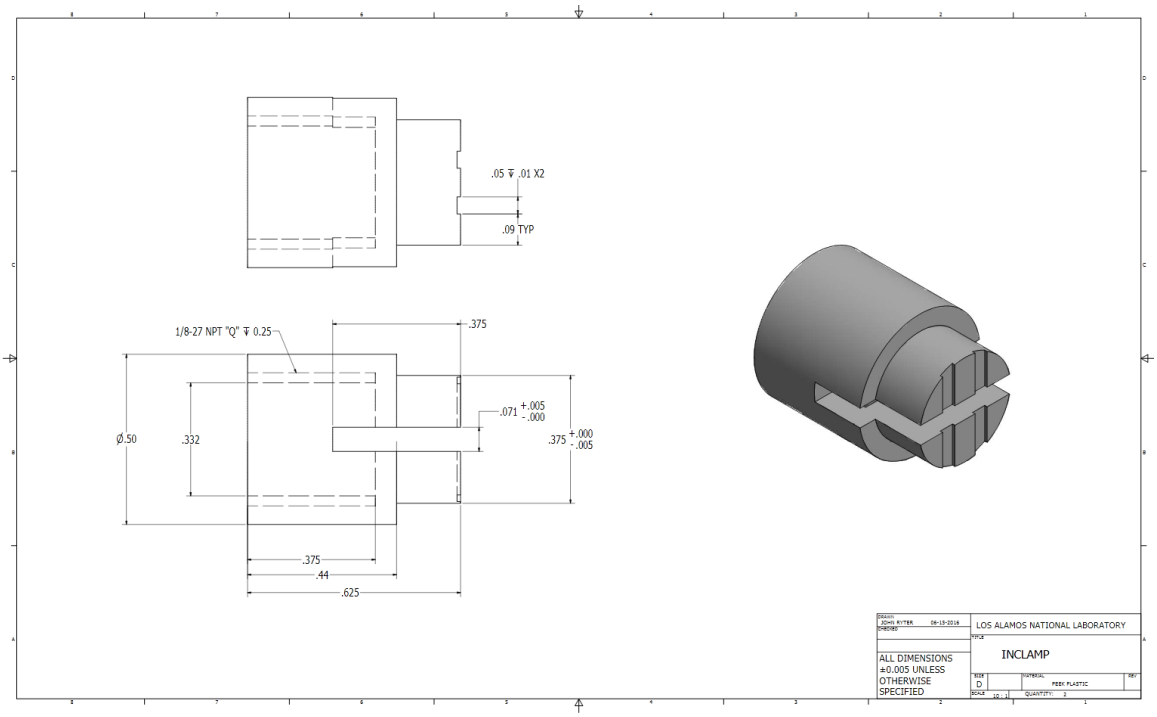


FIG. 3. The sensor holder part drawing used to manufacture the final component. The sensor holder was designed to be flexible enough to allow for compression to take place when the sensor cover was put in place, with that compression being transmitted to the sensor itself to hold it in place.

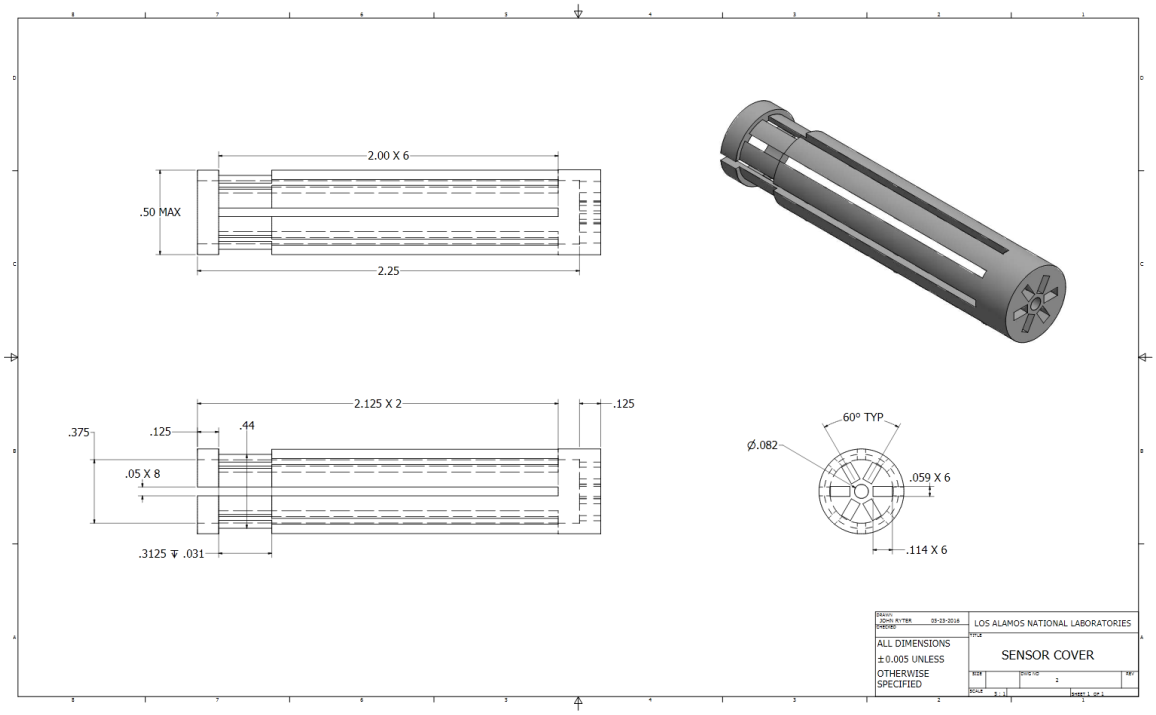


FIG. 4. The sensor cover part drawing used to manufacture the final component. The cover was designed to be compressed over the top of the sensor holder, with this compression holding the assembly together.

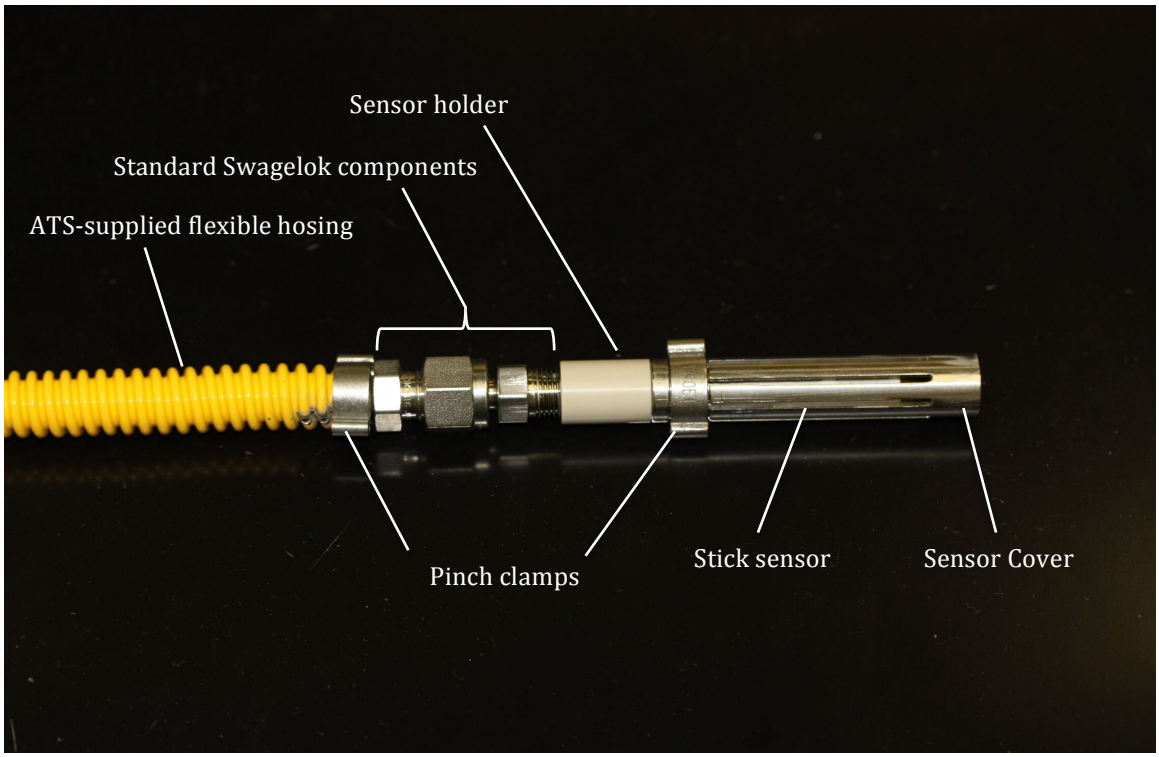


FIG. 5. The final assembly of the automotive sensor and its packaging, with standard Swagelok components and another pinch clamp used to mate with the ATS-supplied flexible hosing.

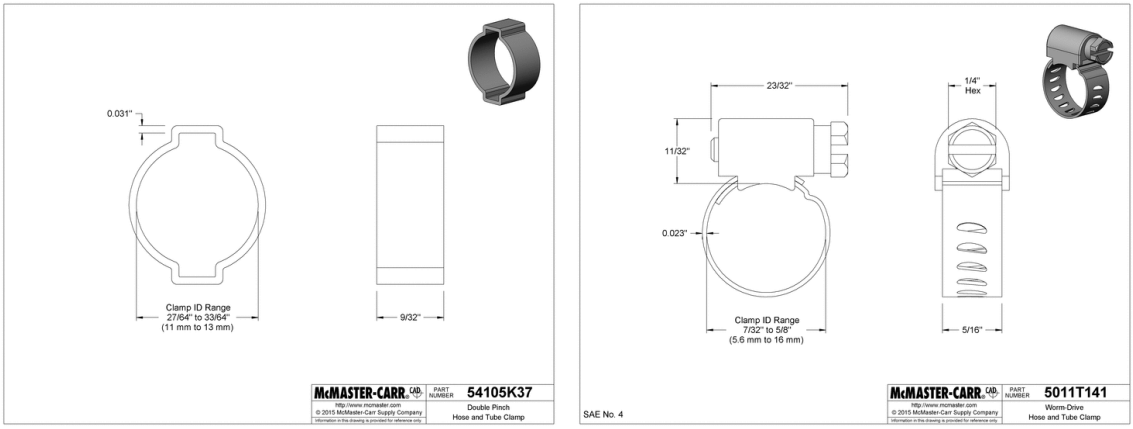


(a) (b)

FIG. 6. (a) The double pinch clamp ordered from McMaster-Carr used to assemble automotive sensor packaging as well as to attach the sensor array to the ATS-supplied flexible tubing. (b) The worm drive clamp was investigated and compared with the double pinch clamp, eventually being removed from consideration due to its bulkiness.

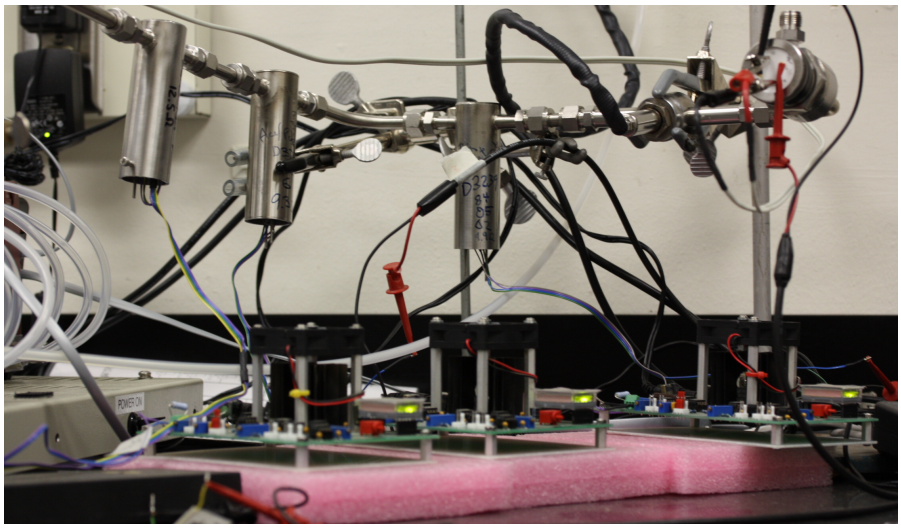

FIG. 7. The sensor array was designed to replace the system shown above, which is currently being used to collect the data required to deconvolute complex gas mixtures. Each sensor is housed in a separate port and requires a separate power supply.

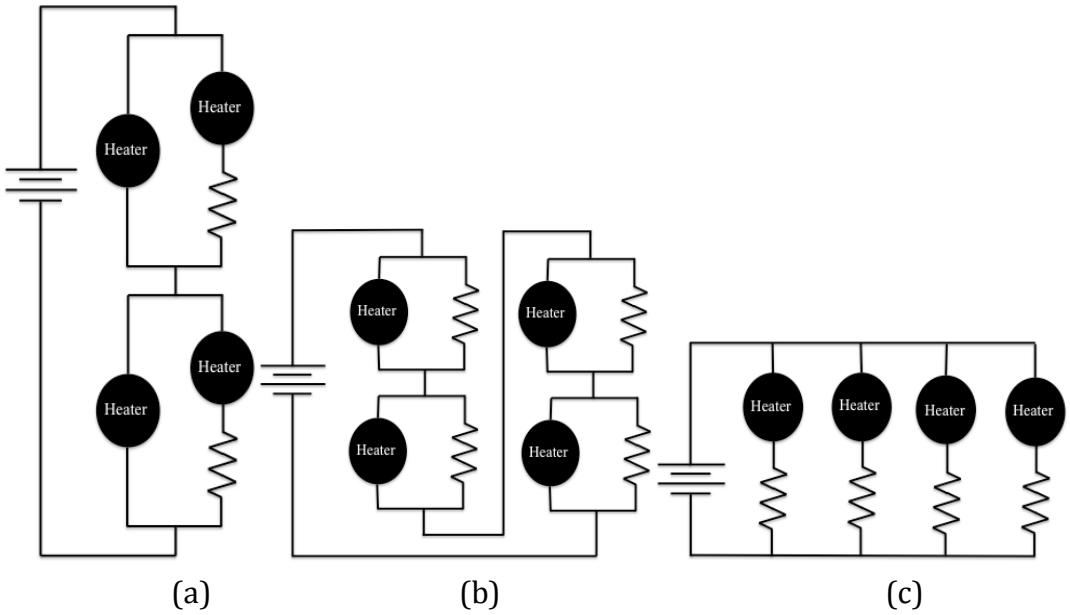


FIG. 8. (a) This design minimized the number of resistors required and provided a balance of voltage and current requirements, both being moderate and within the capacity of the power supply. (b) This design drew less current but had large voltage requirements. (c) This design had smaller voltage requirements but drew a large current.

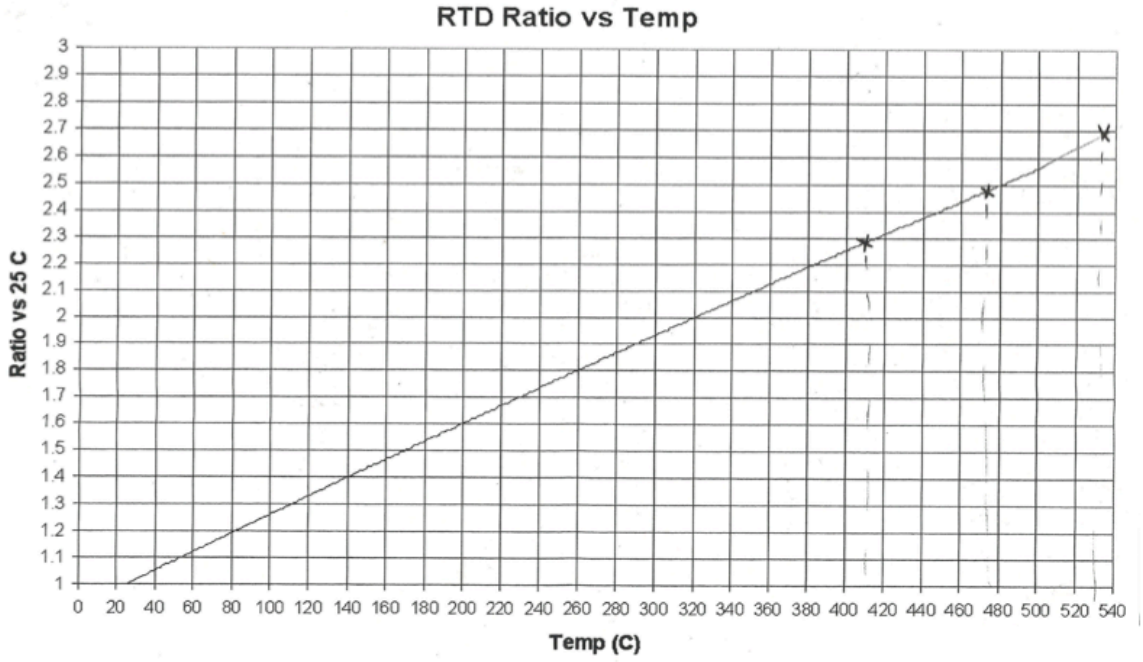


FIG. 9. This plot shows the correlation of the heater resistance ratio to its operating temperature. The resistance ratio is equivalent to the resistance measured under operating conditions (found by dividing the operating voltage by the corresponding current) divided by the nominal resistance, or the heater resistance at 25˚C.

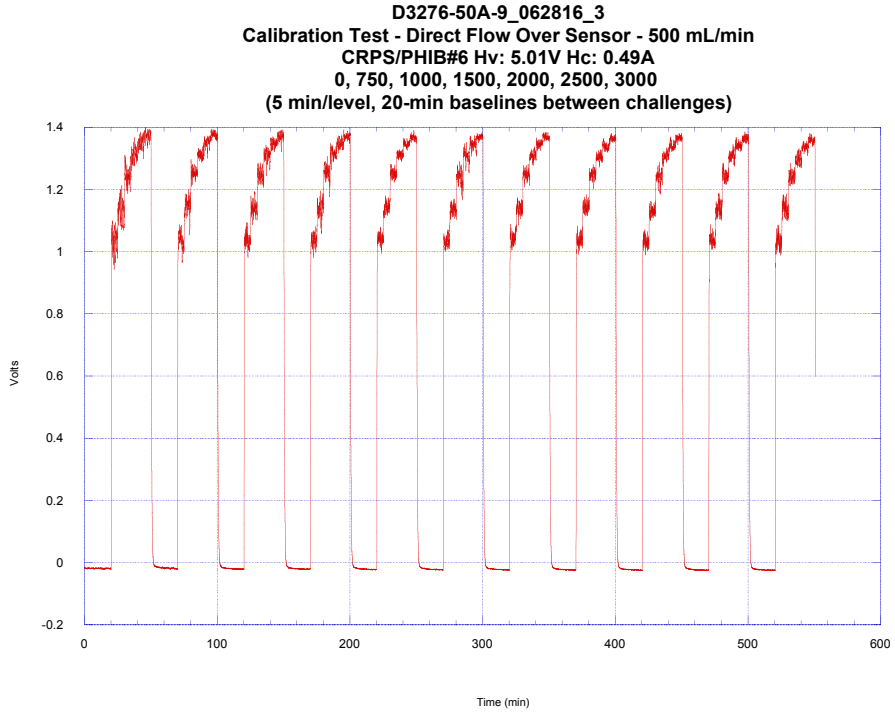


FIG. 10. This figure shows an example of a sensor response to a series of hydrogen staircase challenges. In this case, an ITO sensor with a saturation threshold of 3000 ppm (0.3%) $H_2$ was exposed to a battery of staircases, demonstrating the strong reproducibility of its response.


(a) (b)

FIG. 11. (a) This figure shows the interior of the wall mounted hydrogen sensor field test unit, where the large gray faraday cage enclosing the power supply and the protruding ceramic sensor holder can be seen, along with the wireless data transmitter and the intake fan. (b) This figure shows an external view.

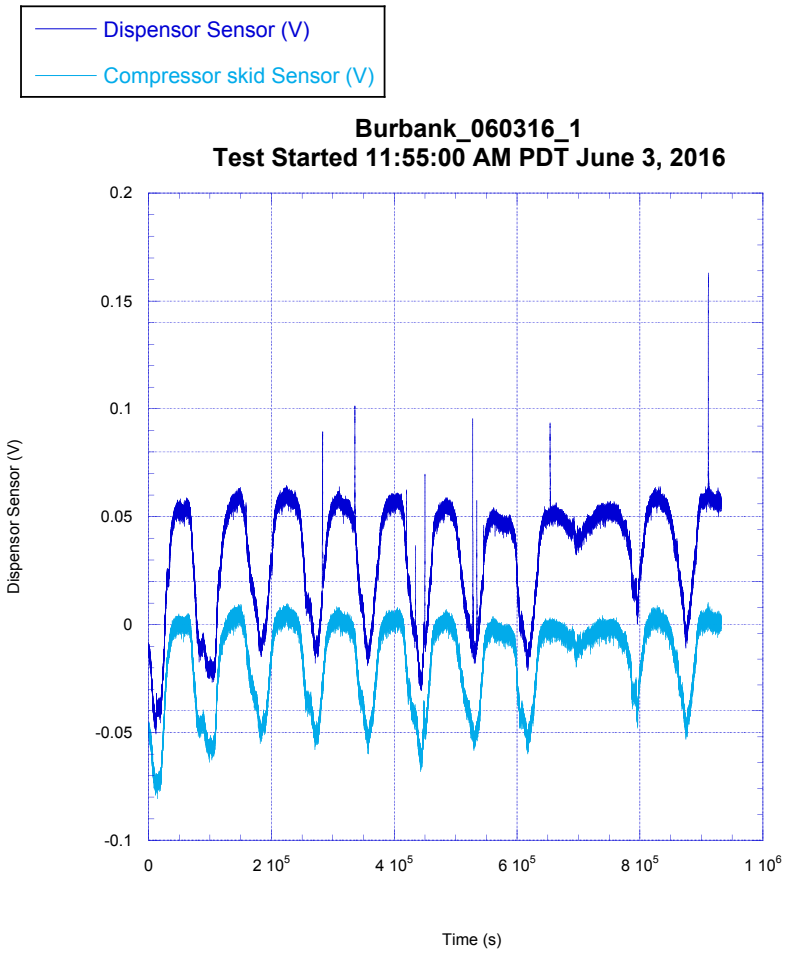


FIG. 12. This figure shows the voltage response of both the dispenser (dark blue) and compressor skid (light blue) sensors over the course of approximately ten days. The baseline drift, on a 24-hour cycle, can be clearly seen, as well as several peaks in the dispenser sensor's response.

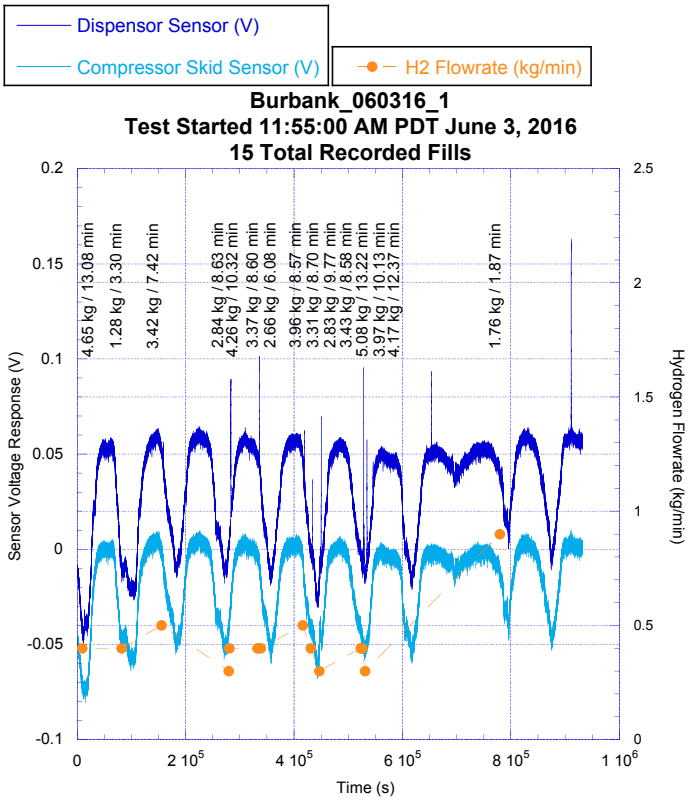


FIG. 13. This figure incorporates data regarding hydrogen vehicle fueling events. The mass and duration of each fueling event is displayed, with the orange points showing the hydrogen flow rate and when the event occurred. Several fueling events were not detected by the sensor, likely due to environmental conditions such as wind direction. The two spikes recorded that do not correlate with fueling events have been attributed to other hydrogen releases at the station.

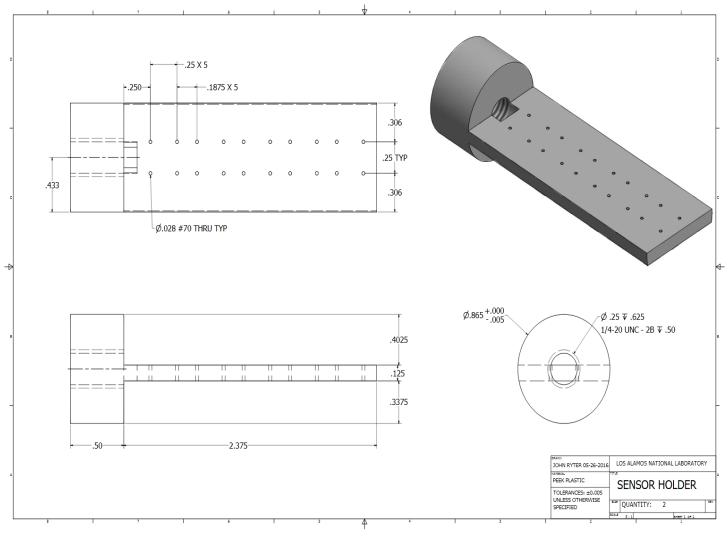


FIG. 14. The sensor array design used to manufacture the final product. The pin holes and threading were designed to incorporate existing components, simplifying the design.

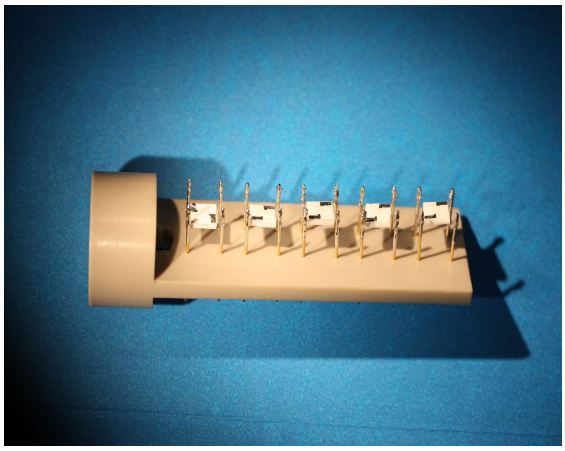

FIG. 15. The sensor array following the mounting of the sensors and pins. A fifth sensor was incorporated into the design to permit greater flexibility in the system.

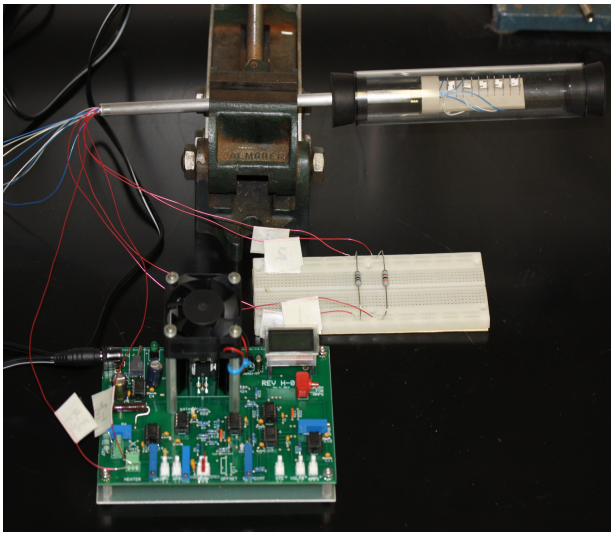

FIG. 16. The final assembly, including the sensor array mounted in quartz tubing, the two resistors required for the completion of the circuit, and the power supply. The two resistors were wired so as to be non-permanent and easily replaceable during the prototyping process

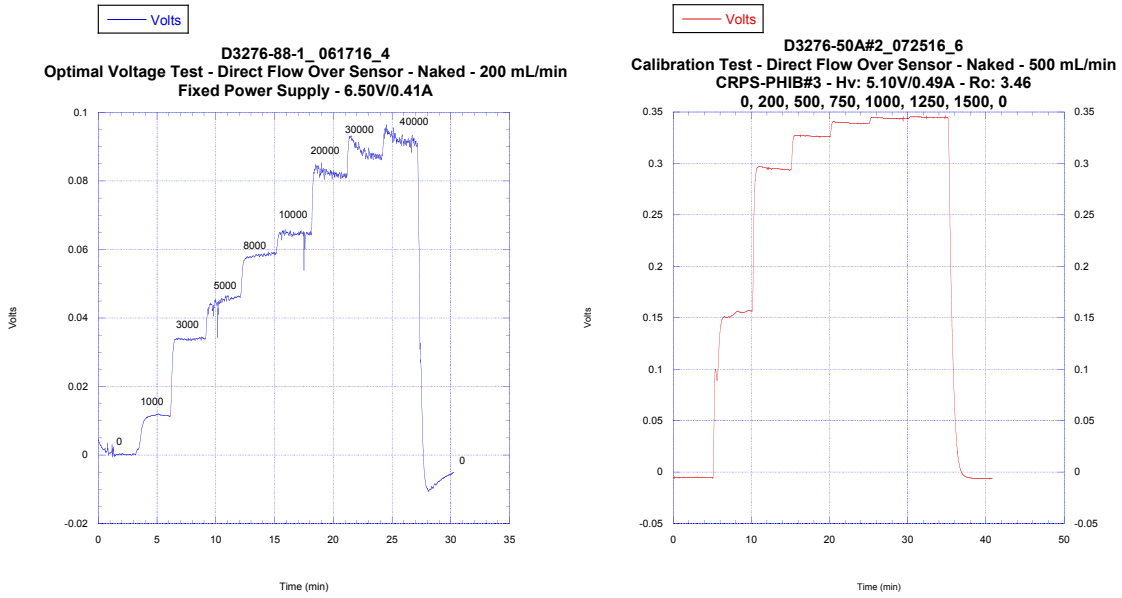


(a) (b)

FIG. 17. (a) This figure shows the voltage response of a lanthanum chromite sensor during a hydrogen staircase challenge, with the saturation threshold appearing at approximately 40,000 ppm (4%) $H_2$. (b) This figure shows the voltage response of an ITO sensor, with its threshold occurring at approximately 1,500 ppm (0.15%) $H_2$.

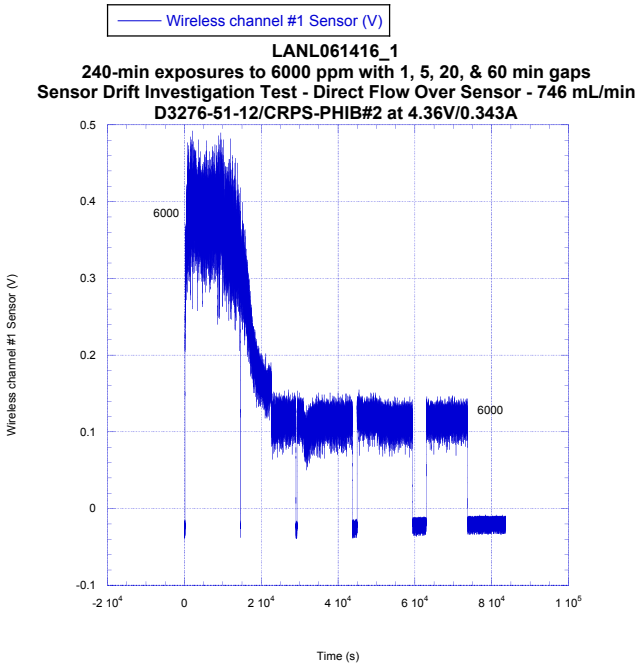


FIG. 18. This figure shows the voltage response of a lanthanum chromite sensor during five 240-minute hydrogen exposures at 6,000 (0.6%) $H_2$, which is well below its saturation threshold. The deterioration of the sensor response can be clearly seen, alongside its lack of recovery.

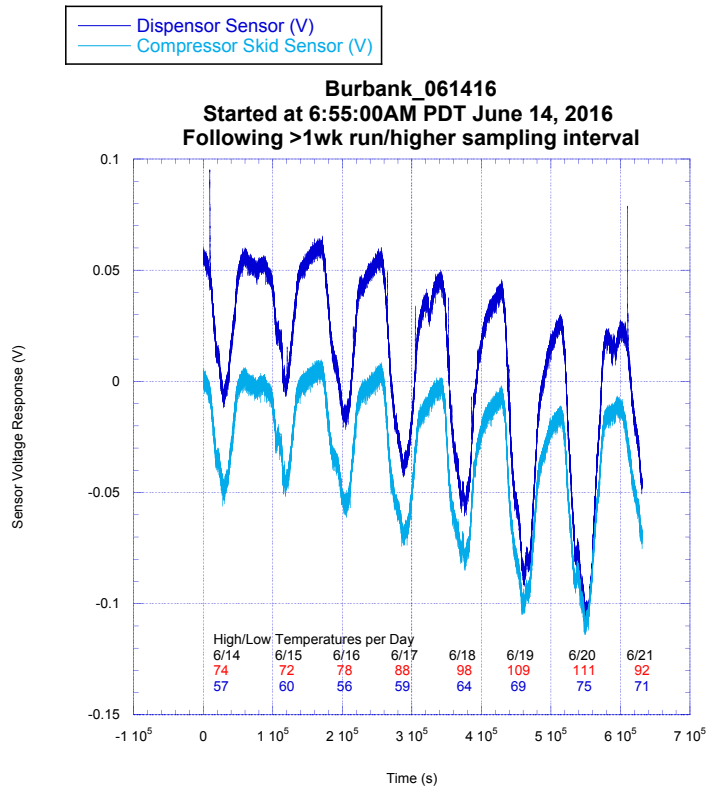


FIG. 19. This figure shows the temperature-induced baseline drift in both sensors undergoing field trials testing in Burbank, California in the presence of extreme temperatures.

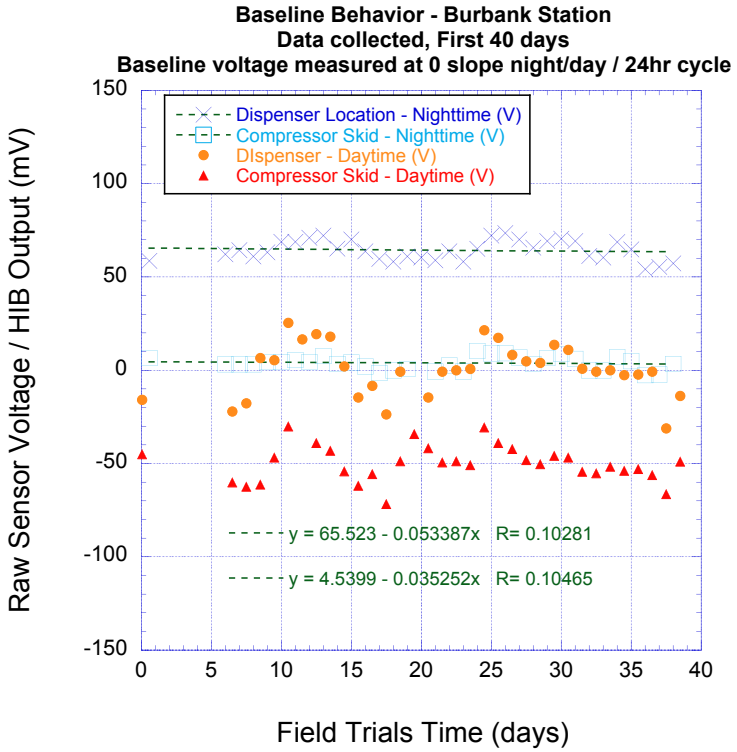


FIG. 20. This figure shows the overall drift of the two field trials sensors at the hydrogen vehicle fueling station in Burbank, California over the course of 40 days. Because of the cyclic drift, the data

points shown above were collected at the maximum and minimum recorded values on each day. The two dashed lines, with slopes approaching zero, show that drift was minimal and possibly negligible.

## Acknowledgements

This work was supported by the U.S. Department of Energy's Laboratory Directed Research and Development (LDRD) program, funding from the state of California, and the Science Undergraduate Laboratory Internship (SULI) program. Dr. Eric Brosha, Christopher J. Romero, Roger Lujan provided mentorship and guidance. Other acknowledgements include: Automotive Test Solutions, the National Renewable Energy Laboratory, Lawrence Livermore National Laboratory, Oak Ridge National Laboratory, Custom Sensor Solutions, and ESL ElectroScience.

---

[1] F.H. Garzon, R. Mukundan and E.L. Brosha, Solid State Ionics 136-137, 633-638 (2000)
[2] J.W. Fergus, Journal of Solid State Electrochemistry 15 (5), 971-984 (2010)
[3] P.K. Sekhar, E.L. Brosha, R. Mukundan, M.A. Nelson, T.L. Williamson and F.H. Garzon., Sensors and Actuators B: Chemical 148.2, 469-477 (2010)
[4] C.R. Kreller, P.K. Sekhar, V.Y. Prikhodko, J.A. Pihl, S.J. Curran, J.E. Parks, R. Mukundan, F.H. Garzon and E.L. Brosha, ECS Transactions 61, 55-63 (2014)
[5] K. Ramaiyan, C.R. Kreller, E.L. Brosha, R. Mukundan, U. Javed, and A.V. Morozov, "Quanititave Decoding of Complex Gas Mixtures Using Mixed-Potential Sensor Arrays," Sensors and Acutators B: Chemical, under review
[6] J.W. Fergus, Journal of Solid State Electrochemistry 15 (5), 971-984 (2010)
[7] M.D. Nathanson, Patent: US6263268 B1 (2001)
[8] F.H. Garzon, R. Mukundan and E.L. Brosha, Solid State Ionics 136-137, 633-638 (2000)
[9] K. Ramaiyan, C.R. Kreller, E.L. Brosha, R. Mukundan, U. Javed, and A.V. Morozov, "Quanititave Decoding of Complex Gas Mixtures Using Mixed-Potential Sensor Arrays," Sensors and Acutators B: Chemical, under review
[10] J. Tsitron, C.R. Kreller, P.K. Sekhar, R. Mukundan, F.H. Garzon, E.L. Brosha, and A.V. Morozov, Sensors and Actuators B: Chemical 192, 283-293 (2014)
[11] P.K. Sekhar, E.L. Brosha, R. Mukundan, M.A. Nelson, T.L. Williamson and F.H. Garzon., Sensors and Actuators B: Chemical 148.2, 469-477 (2010)
[12] D.P. Jones, D.C. Leach, and D.R. Moore, Polymer 26.9, 1385-1393 (1985)